e-J. Surf. Sci. Nanotech. Vol. 16 (2018) 193-200 Conference - ISSS-8 -

Adsorption and Diffusion Properties of a Single Iron Atom on Light-Element-Doped Graphene*

Shun Hasegawa, Yuji Kunisada,† and Norihito Sakaguchi
Center for Advanced Research of Energy and Materials, Hokkaido University, Kita 13, Nishi 8, Kitaku, Sapporo, Hokkaido 060-8628, Japan
(Received 9 January 2018; Accepted 25 April 2018; Published 25 May 2018)

In this study, we calculated the diffusion of an Fe atom on graphene and various light-element (B, N, O, Si, P, and S)-doped graphene supports, using first-principles calculations based on density functional theory. We focused on dopants that could suppress the detachment and diffusion of an Fe atom. Such doped graphene supports would have strong potential in high-durability fuel cell catalysts and hydrogen storage materials. The Fe atom adsorbs on pristine graphene via ionic bonding. The bonding between the Fe atom and pristine graphene is very weak, and it has a low adsorption energy of −0.61 eV. Doped graphene contains unoccupied localized orbitals. B-, O-, Si-, and P-doped graphene show high adsorption energies of −1.70 eV, −2.70 eV, −1.46 eV, and −1.38 eV, respectively. Thus, these graphene supports could suppress the detachment of Fe nanoclusters and nanoparticles. We demonstrate that these doped graphene supports with high adsorption energies also have high diffusion barriers, which suppresses the agglomeration of Fe nanoclusters and nanoparticles. We conclude that B-, O-, Si-, and P-doped graphene are promising supports for enhancing the adsorption lifetime of Fe nanoclusters and nanoparticles.
[DOI: 10.1380/ejssnt.2018.193]

Keywords: Density functional calculations; Iron; Carbon; Surface diffusion

I. INTRODUCTION

Iron is one of the most important elements in various engineering and scientific fields, because of its many useful properties. Structural materials are commonly made from steels, because of their abundance, high workability, and high corrosion resistance. Iron also plays an important role as catalysts, for instance, in the Haber-Bosch process.

Fe nanoclusters and nanoparticles have attracted much recent interest as catalysts in astrochemistry, and in hydrogen energy devices in materials science. Iron is one of the most abundant transition metals in space and on earth. Fe atoms, nanoclusters, nanoparticles, and their oxides on carbon materials and ice, which are the main components of interstellar clouds and cosmic dust, may be catalysts for the evolution of organic molecules.

The efficient and safe storage of hydrogen is an important problem to solve for achieving widespread fuel cell commercialization [1]. For practical applications, hydrogen storage materials require high gravimetric density, high volumetric density, and a high degree of safety. Non-precious metal atom Li [2], Al [3] and transition elements including Fe nanoclusters [4, 5] were recently reported to exhibit high efficiency hydrogen storage. For instance, Fe_2 clusters can reportedly store up to 18 H atoms [6]. However, bulk Fe hydride cannot be synthesized under ambient pressure, instead requiring pressures of 3.5 GPa [7–10]. Theoretical and experimental results have shown that Fe cluster hydrides can adsorb in a stable manner on graphene supports [11, 12]. Several studies have also reported that Fe nanoparticle/graphene composites show high catalytic activity for the oxygen reduction reaction (ORR), which is the cathode reaction in fuel cells [13, 14]. Expensive Pt nanoparticles are currently usually used in fuel cells as ORR catalysts. Developing low-cost and more abundant catalysts such as Fe nanoparticles is necessary for fuel cell popularization.

The size of Fe nanoclusters and nanoparticles is crucial for their catalytic activities and hydrogen storage properties. To understand the process of the evolution of organic molecules in space, the diffusion and agglomeration properties of Fe atoms requires clarifying. In addition, to develop long-life hydrogen storage materials and catalysts, the diffusion and agglomeration of Fe atoms needs to be suppressed. The planar structure and delocalized π-electrons of graphene rarely form strong covalent bonding with adsorbates. This means that adsorbates can detach or diffuse from the basal plane to the edges where dangling bonds exist, which results in the loss or agglomeration of adsorbates. Chemical modification of the graphene lattice by heteroatom doping is a common way to form anchor sites in graphene. The N-doping of graphene supports can reportedly increase the dispersion of Pt catalysts [15] and prevent Pt agglomeration [16, 17]. This improves the catalyst durability and efficiency for the ORR, compared with that of pristine graphene supports. The S-doping of graphene can also increase the efficiency of ORR via the same mechanism [18]. Thus, doping graphene supports with light elements can suppress the diffusion and agglomeration of adsorbates. However, it remains unclear how the dopants affect the adsorption state and diffusion behavior of Fe atoms.

In this study, we investigate candidates as dopants for graphene-related supports, to suppress Fe detachment and agglomeration. We investigate the adsorption energy and adsorption configuration of a single Fe atom on various types of light-element-doped graphene, using first-principles calculations based on spin-polarized density functional theory (DFT). We also investigate the corresponding Fe diffusion behavior using nudged elastic band (NEB) calculations.

* This paper was presented at the 8th International Symposium on Surface Science, Tsukuba International Congress Center, Tsukuba, Japan, October 22-26, 2017.
† Corresponding author: kunisada@eng.hokudai.ac.jp

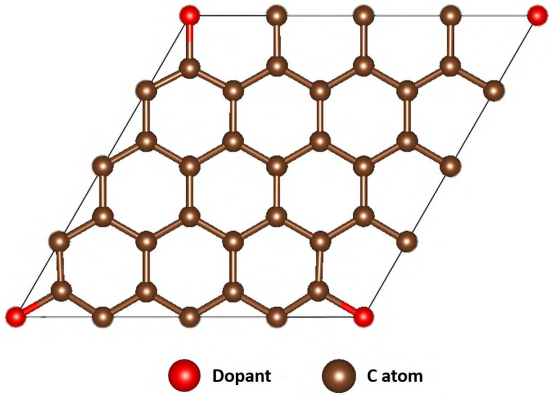

FIG. 1. Atomic configuration of the light-element-doped graphene supercell considered in this study. Brown and red balls indicate C and dopant atoms, respectively.

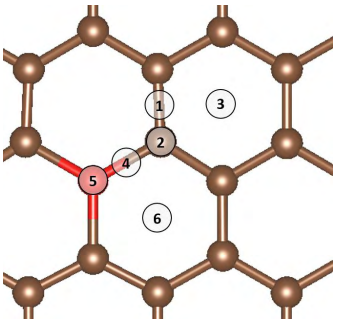

FIG. 2. Initial adsorption sites of Fe atoms on graphene supports. The sites considered include (1) C–C bridge, (2) on top of C, (3) hollow, (4) X–C bridge, (5) on top of X, and (6) X hollow sites. For pristine graphene, the sites considered are (1) C–C bridge, (2) on top of C, and (3) hollow sites. Brown and red balls indicate C and dopant atoms, respectively.

II. COMPUTATIONAL METHODS

DFT calculations were performed to investigate the adsorption and diffusion properties of Fe atoms on light-element-doped graphene, using the Vienna *ab initio* Simulation Package (VASP 5.4.1) [19–22] with the projector-augmented wave (PAW) [23, 24] method. The generalized gradient approximation (GGA) proposed by Perdew, Buke, and Emzerhof (PBE) [25] was adopted to describe the exchange-correlation functional. An energy cutoff of 500 eV for a plane-wave basis set was used. The supercell consisted of a 4×4 graphene monolayer and a 15-Å-wide vacuum layer with a periodic boundary condition. We introduced the dopant atom by substitution of a single carbon atom in the graphene lattice, as shown in Fig. 1. The concentration of the dopant was 3.1 at.%. To reveal the dopant dependence of the Fe adsorption and diffusion, we investigated six light-element dopants (X), where X = B, N, O, Si, P, and S. We used a $4 \times 4 \times 1$ Γ-point centered MonkhorstPack grid [26] for Brillouin zone sampling to calculate the total energy, with a Gaussian smearing σ of 0.2 eV. All atoms were fully relaxed until the force on each atom was less than 0.02 eV/Å. We used the optimized lattice parameters for the pristine, B-, N-, O-, Si-, P-, and S-doped graphene reported previously [27], and these values are 2.480, 2.462, 2.462, 2.487, 2.492, 2.481, and 2.479 Å, respectively.

We considered three Fe adsorption sites on pristine graphene, namely, at the C–C bridge, on top of C, and at a hollow of the lattice. For X-doped graphene we considered six Fe adsorption sites, namely, at the C–C bridge, at the X–C bridge, on top of C, on top of X, at a C hollow, and at an X hollow. These sites are shown in Fig. 2.

The Fe adsorption energy on X-doped graphene can be written as:

$$E_{\mathrm{ab}}^{\mathrm{X}} = E_{\mathrm{Fe-gra}}^{\mathrm{X}} - \left(E_{\mathrm{gra}}^{\mathrm{X}} - \mu_{\mathrm{Fe}}\right), \qquad (1)$$

where $E_{\mathrm{Fe-gra}}^{\mathrm{X}}$ and $E_{\mathrm{gra}}^{\mathrm{X}}$ are the total energy of the X-doped graphene with and without Fe atoms, and μ_{Fe} is the chemical potential of Fe which is defined as the energy of a single isolated Fe atom in vacuum.

We calculated the Fe diffusion paths and diffusion barriers on pristine and light-element-doped graphene using the NEB method. We considered diffusion from the most stable adsorption sites to nearest neighbor metastable adsorption sites. The spring constant was 5.0 eV/Å^2. All atoms were fully relaxed until the total force on each atom was less than 0.02 eV/Å. The Brillouin zone sampling was conducted with a $3 \times 3 \times 1$ Γ-point centered MonkhorstPack grid for the NEB calculations.

To compensate for the dipole-dipole interaction between graphene layers, a dipole moment correction was incorporated [28, 29]. We calculated the electron transfer by using Bader charge analysis [30–32]. We also calculated the crystal orbital Hamilton population (COHP) using the LOBSTER package [33, 34]. We used Visualization for Electronic and Structure Analysis (VESTA) for visualizing atomic models and electron density distributions [35].

III. RESULTS AND DISCUSSION

We first investigated the most stable adsorption states of Fe atoms on pristine and light-element-doped graphene. Table I shows calculated Fe adsorption energies and corresponding magnetic moments at the most stable adsorption sites on pristine and light-element-doped graphene. Table I shows that all dopants considered in this study

TABLE I. Adsorption energies at the most stable adsorption sites of Fe atoms on pristine and light-element-doped graphene, and magnetic moments of the corresponding systems.

Dopant	Adsorption energy (eV)	Magnetic moment (μ_{B})
pristine	−0.61	2.05
B	−1.70	2.98
N	−0.76	1.86
O	−2.70	2.01
Si	−1.46	3.55
P	−1.38	3.00
S	−0.84	2.04

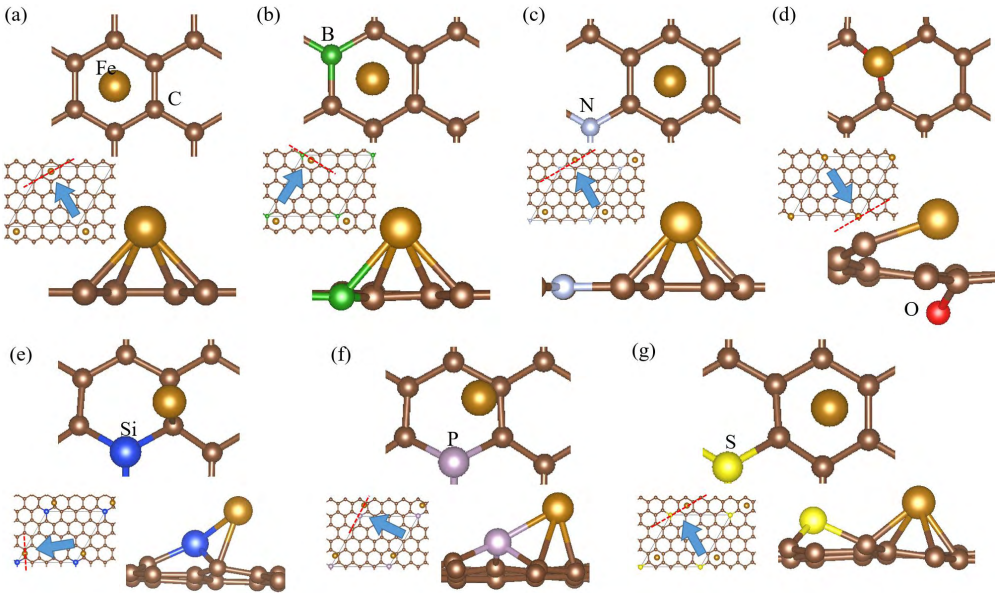

FIG. 3. The most stable atomic configuration of Fe atoms on (a) pristine graphene and (b) B-, (c) N-, (d) O-, (e) Si-, (f) P-, and (g) S-doped graphene. Illustrations above and below show top and side views of the structure, respectively. The side view shows a plane in the plane indicated by the dashed lines and arrows in the insets. Brown, green, grey, red, blue, purple, yellow, and gold balls indicate C, B, N, O, Si, P, S, and Fe atoms, respectively.

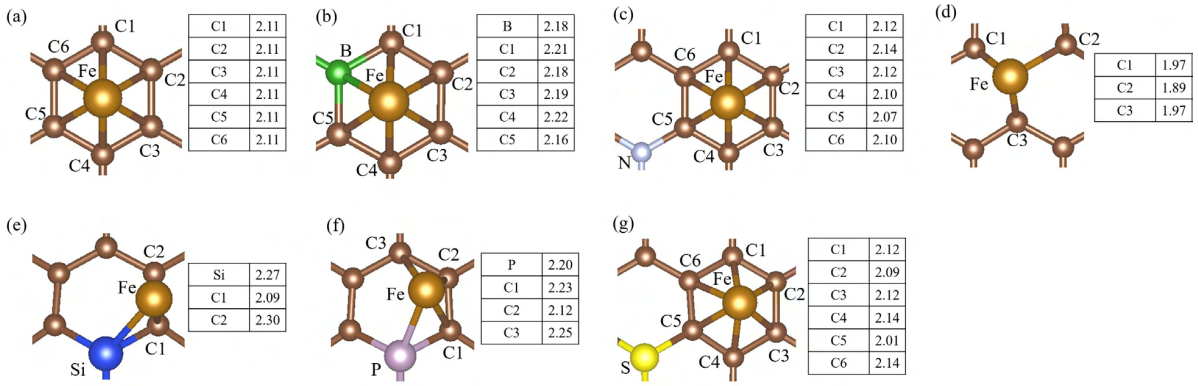

FIG. 4. The bond lengths between Fe and coordinated atoms in (a) pristine, (b) B-, (c) N-, (d) O-, (e) Si-, (f) P-, and (g) S-doped graphene. The tables beside the atomic configurations show the bond lengths between Fe atom and each atom labeled in atomic configurations. The unit is Å.

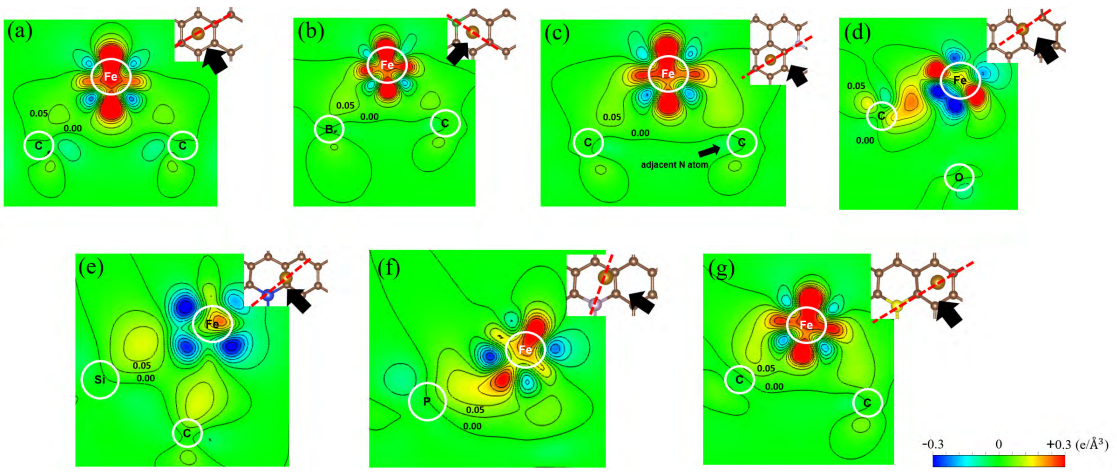

FIG. 5. Adsorption-induced electron density difference in the vicinity of Fe atoms on (a) pristine graphene and (b) B-, (c) N-, (d) O-, (e) Si-, (f) P-, and (g) S-doped graphene. The contour line interval is 0.05 e/Å^3.

increase the adsorption energies of the Fe atom. The adsorption energy of the Fe atom decreases in the order: O- > B- > Si- > P- > S- > N-doped graphene. These adsorption energies indicate that B-, O-, Si-, and P-graphene are promising candidates for catalyst supports, in which suppression of Fe detachment is required to increase the lifetime of Fe/graphene composites. Figure 3 shows top and side views of the most stable atomic configurations of Fe atoms on pristine and light-element-doped graphene. The most stable adsorption site of an Fe atom on pristine graphene is consistent with previous theoretical reports [36–38]. Figure 3 shows that Fe atoms tend to adsorb at high-coordination-number sites. The bond length between Fe atom and atoms in pristine and doped-graphene are shown in Fig. 4. We found that, in the cases of Fe adsorption at hollow sites, the bond lengths between Fe and coordinated atoms only slightly vary. Next, we investigated the origin of dopant effect on Fe adsorption from electronic states by using projected density of states (PDOS), Bader analysis, electron density difference before and after Fe adsorption and COHP.

We discuss the origin of the dopant effect on Fe adsorption. We calculated the adsorption-induced electron density difference in the vicinity of Fe atoms on pristine and light-element-doped graphene. The results are shown in Fig. 5. Figure 5(a) shows that there is no strong covalent bond between Fe and the C atoms of pristine graphene. Additionally, the PDOS of the Fe and C atoms are shown in Fig. 6(a). The PDOS does not show any peaks in the same energy range. We then calculated the COHP, as shown in Fig. 7. Figure 7(a) does not show any clear positive peak below the Fermi level, which would indicate bonding orbitals. From these results, we conclude that an Fe atom on pristine graphene does not form covalent bonds with coordinated C atoms. To reveal the adsorption state of an Fe atom on pristine graphene, we evaluated the valance numbers of the Fe atom and C atoms in pristine graphene using Bader charge analysis. Figures 8 and 9 show Bader charge of each atom before and after Fe adsorption, respectively. Figure 8(a) shows that the Bader charge of C atoms in pristine graphene before Fe atom adsorption is nearly zero. After Fe adsorption, the Bader charge of C atoms coordinated with an Fe atom become negative, with an average Bader charge of −0.11. The Bader charge of Fe is +0.67. This means that electrons transfer from the Fe atom to the coordinated C atoms. Figure 10 shows the PDOS of s orbitals in an Fe atom before and after adsorption on pristine graphene. The PDOS of the s orbitals moves above the Fermi level, after Fe adsorbs on pristine graphene. This indicates electron transfer from the s orbital of the Fe atom to the coordinated C atoms. Figure 5(a) also indicates electron transfer from the Fe to C atoms, and electron redistribution in the Fe atom induced by the coordinated negatively-charged C atoms. Thus, we conclude that the Fe atom adsorbs on pristine graphene via ionic bonding. The small electron transfer of 0.67 results in a small adsorption energy of −0.61 eV, as shown in Table I.

The Fe atom adsorbs strongly on B-doped graphene, whose adsorption energy is −1.70 eV, as shown in Table I. This is despite the Fe atom adsorbing at hollow sites in the same manner as that for pristine graphene. Figure 8(b) shows that B atoms in B-doped graphene are positively charged. C atoms coordinated with a B atom (C_B) are negatively charged, because of the differing electronegativities of B and C. We calculated the Coulomb interaction between Fe atoms at B-hollow sites, and found that the attractive (Fe–C) and repulsive (Fe–B) Coulomb interactions almost cancel. Thus, an Fe atom cannot adsorb on B-doped graphene through Coulomb interaction, in contrast to pristine graphene. This unequally distributed electron in the vicinity of the B atom breaks the symmetry of the system, and creates localized p_z orbitals in the B and C_B atoms. These orbitals may strongly hybridize with the electrons of the Fe atom. The adsorption-induced difference in electron densities of the Fe and B atoms is slightly higher than the adsorption-induced difference in electron densities of the Fe and C atoms for adsorption on pristine graphene, as shown in Fig. 5(a, b). To further investigate the Fe adsorption states on B-doped graphene, we investigated the PDOS and COHP of B-doped graphene, as shown in Figs. 6(b) and 7(b). The PDOS of Fe and B both show clear peaks from −4 eV to −2 eV. A positive peak of COHP is also observed in the same energy region of the PDOS analysis. These results indicate that Fe and B atoms form covalent bonds through Fe d and unoccupied B p_z orbitals. Similar positive peaks from the Fe and C_B atoms can be seen in Fig. 7(b). Thus, the Fe atom covalently bonds with C_B more strongly than the ionic bonding of the Fe atom with the C atoms of pristine graphene. We conclude that the Fe atom adsorbs on B-doped graphene through covalent bonds with B and C_B atoms, and has a large adsorption energy of −1.70 eV.

For N-doped graphene, the Fe atom adsorbs at the hollow sites not surrounded by N atoms. Figure 8(c) shows that the N atoms are negatively charged, because the electronegativity of N is higher than that of C. Therefore, N doping introduces positive charge and partially unoccupied p_z orbitals into C atoms adjacent to an N atom (C_N). More electron transfer from the Fe to C_N atoms occurs, compared to in the case of pristine graphene. Figure 5(c) indicates that more electrons localize between the Fe and C_N atoms than the opposite side, i.e., between the Fe and C atoms, or in the case of pristine graphene. The corresponding PDOS and COHP between the Fe and C_N atoms look similar to those of pristine graphene, as shown in Figs. 6(c) and 7(c). However, there is a slight positive peak of the COHP between the Fe and C_N atoms from −3 eV to −1.5 eV. This indicates an increase in the covalent bonding between the Fe and C atoms, as a result of N doping. The electron transfer from the Fe atom to N-doped graphene is 0.47, which is smaller than that on pristine graphene (0.61), because the electrons density of overall system of N-doped graphene increases upon N doping. From these results, we conclude that covalent bonds between the Fe and C_N atoms are formed by N doping, while ionic bonds between the Fe and C atoms weaken. The total adsorption energy of the Fe atom on N-doped graphene is slightly larger than that on pristine graphene.

Strong covalent bonds can be observed for O-, Si- and P-doped graphene, as shown in Figs. 5(d), 5(e), and 5(f), respectively. In O-doped graphene, the C atom adjacent to O (C_O) has dangling bonds, which allow the Fe atom to form strong covalent bonds with C_O. This covalent bond between the Fe and C_O atoms appears as a peak

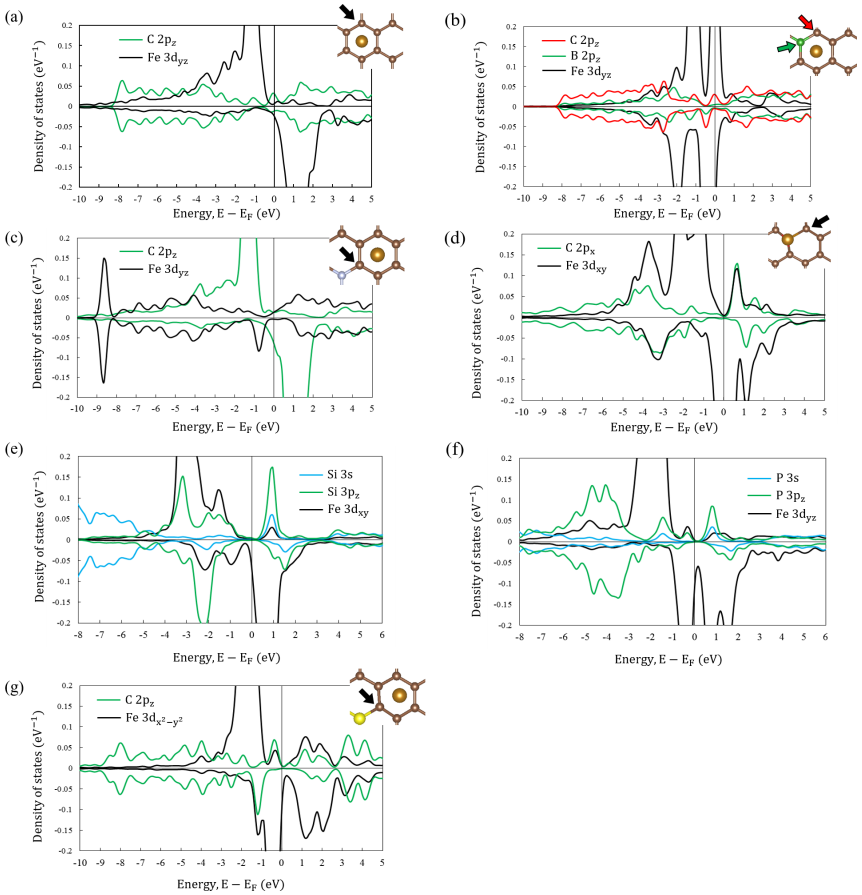

FIG. 6. Projected density of states for Fe atoms adsorbed on (a) pristine graphene and (b) B-, (c) N-, (d) O-, (e) Si-, (f) P-, and (g) S-doped graphene. The energy origin is set to the Fermi energy. The arrows in inset figures denote the atom which we considered. Positive and negative values of the density of states denote orbitals of up spin and down spin respectively.

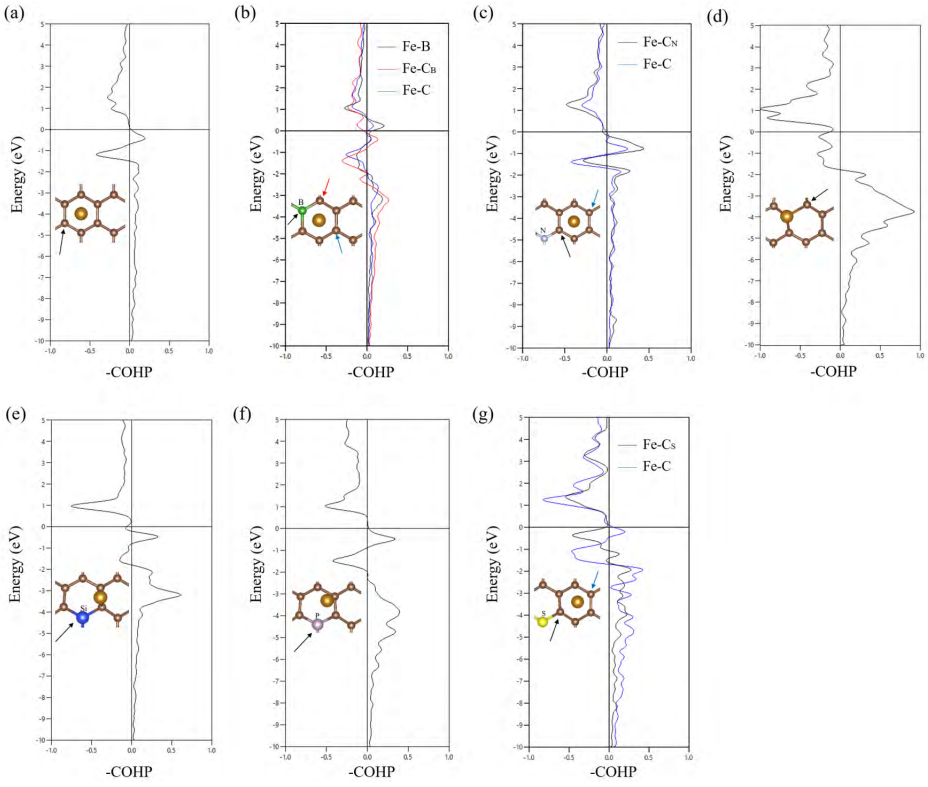

FIG. 7. Crystal orbital Hamilton population (COHP) of (a) pristine graphene and (b) B-, (c) N-, (d) O-, (e) Si-, (f) P-, and (g) S-doped graphene. The energy origin is set to the Fermi energy. The arrows in inset figures denote the atom which we considered.

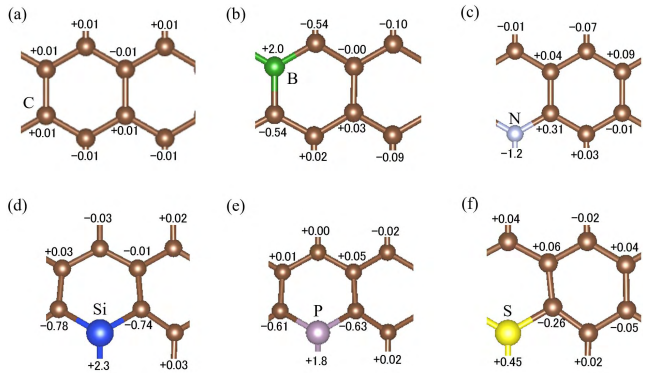

FIG. 8. Bader charge of each atom in (a) pristine graphene and (b) B-, (c) N-, (d) Si-, (e) P-, and (f) S-doped graphene before Fe atom adsorption, as obtained from Bader analysis.

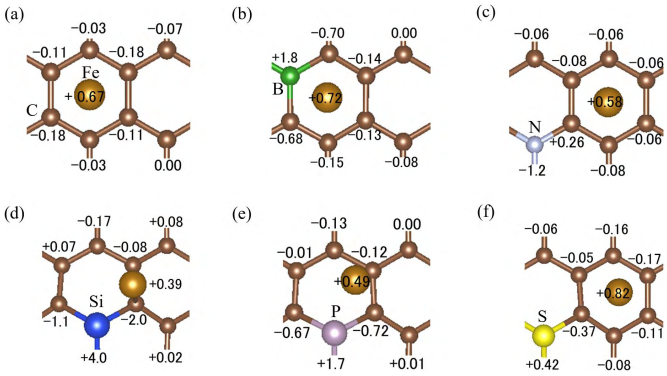

FIG. 9. Bader charge of each atom in (a) pristine graphene and (b) B-, (c) N-, (d) Si-, (e) P-, and (f) S-doped graphene after Fe atom adsorption, as obtained from Bader analysis.

from −4.5 eV to −2.5 eV below the Fermi level in both the PDOS and COHP, as shown in Figs. 6(d) and 7(d), respectively. Thus, the Fe atom on O-doped graphene shows a large adsorption energy. Si and P atoms form protruding configurations, as seen in Figs. 3(e) and 3(f), respectively. These protruding configurations break the sp^2 hybrid orbitals of pristine graphene, and introduce sp^3 hybrid orbitals in the vicinity of the dopant. Si and P atoms coordinate with only three C atoms. Therefore, one sp^3 hybrid orbital remains as a dangling bond, which allows strong covalent bonds to form with the Fe atom, as shown in Figs. 5(e) and 5(f), respectively, even though the repulsive interaction between Fe and Si, P atom exist as shown in Fig. 9(d, e). Figures 8(e) and 8(f) show that the Si and P atoms are positively charged, respectively. This indicates that partially unoccupied sp^3 hybrid orbitals exist within the Si and P atoms [27]. Figures 6(e) and 6(f) show the PDOS of Si- and P-doped graphene, respectively. Figure 6(e) shows that the PDOS of the Fe $3d_{xy}$ and Si sp^3 hybrid orbitals have peaks from −4 eV to −1 eV below the Fermi level. Figure 6(f) shows that the Fe $3d_{yz}$ and P sp^3 hybrid orbitals also have peaks from −5 eV to −3 eV below the Fermi level. These peaks are bonding orbitals between the Fe atom and dopant, as shown in Fig. 7(e, f). These results indicate that Fe atoms form strong covalent bonds with Si and P atoms, resulting in large Fe atom adsorption energies of 1.46 eV and 1.38 eV, respectively.

S atoms also protrude out of the graphene plane, as well as the dopants of Si- and P-doped graphene. However, the adsorption energy of the Fe atom on S-doped graphene is much smaller than those on Si- and P-doped graphene, as shown in Table I. This is because the S atom prior to adsorption has six valance electrons. Figure 8(f) indicates that the Bader charge of S atom is 0.45, indicating that little unoccupied sp^3 hybrid orbitals exist within the S atom [27]. Fe cannot form covalent bonds with the S atom, and very little electron transfer from Fe to S occurs. Thus, the adsorption energy of the Fe atom on S-doped graphene (−0.84 eV) is smaller than those of the Fe atom on Si- and P-doped graphene. This situation is similar to the case of N-doped graphene. In both N- and S-doped graphene, the Fe atom adsorbs at hollow sites coordinated only with C atoms. Figure 9(f) shows that little electron transfer occurs from the Fe to C atoms in the vicinity of Fe atom compared with pristine graphene because the electron density of overall system of S-doped graphene increases upon S doping, which results in weak ionic bonds. The C atoms adjacent to the S atom (C_S) also breaks the sp^2 hybrid orbitals, because the C_S atoms slightly protrude out of the graphene plane, as shown in Fig. 3(g). Therefore, C_S atoms can form covalent bonds with the Fe atom, as seen in Fig. 5(g). The PDOS and COHP between the Fe and C_S atoms are similar to those for pristine graphene, as shown in Figs. 6(a, g) and 7(a, g). Therefore, we conclude that covalent bonds between the Fe and C_S atoms are very weak.

We also investigated the diffusion behaviors of Fe atoms on pristine and light-element-doped graphene. Figure 11 shows the potential energy changes along the diffusion paths that Fe atoms migrate from the most stable adsorption state to metastable adsorption states. The metastable adsorption states have a similar adsorption energy as pristine graphene. The data in Fig. 11 was obtained from NEB calculations. We note that the Hellmann-Feynman forces on Fe atoms at the transition states in all systems are less than 0.03 eV/Å, which indicates that we could reach the accurate saddle points. The diffusion barriers of Fe atoms on light-element-doped graphene increase in the order of N-, S-, B-, P-, Si-, and O-doped graphene. The diffusion barriers of Fe atoms on light-element-doped graphene are all larger than that on pristine graphene. This indicates that all the dopants suppress Fe diffusion. Figure 11 shows that dopants leading to a large adsorption energy of the Fe atom also lead to high diffusion barriers for the Fe atom. This indicates that the origin of the diffusion barrier originates from the large adsorption energy, i.e., a deep potential well in the vicinity of the dopant. This trend has also been reported for Pt diffusion on light-element-doped graphene [27]. Pristine, N-, and S-doped graphene have small adsorption energies for the Fe atom, and this may lead to the agglomeration and degradation of Fe sub-nanoclusters. B-, O-, Si-, and P-doped graphene have large diffusion barriers of 0.97, 2.12, 1.16, and 1.04 eV, respectively, so can maintain the Fe sub-nanocluster size and their physical properties for a long time. The corresponding diffusion barriers from the metastable adsorption sites to the most stable adsorption sites on the doped graphene supports considered in this study are all smaller than those in the opposite direction.

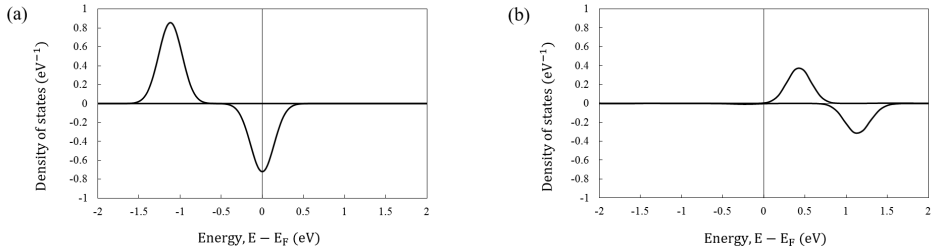

FIG. 10. PDOS of s orbitals of an Fe atom (a) isolated in vacuum and (b) adsorbed on pristine graphene. The origin of energy is set to the Fermi energy. Positive and negative values of the PDOS denote orbitals of up spin and down spin respectively.

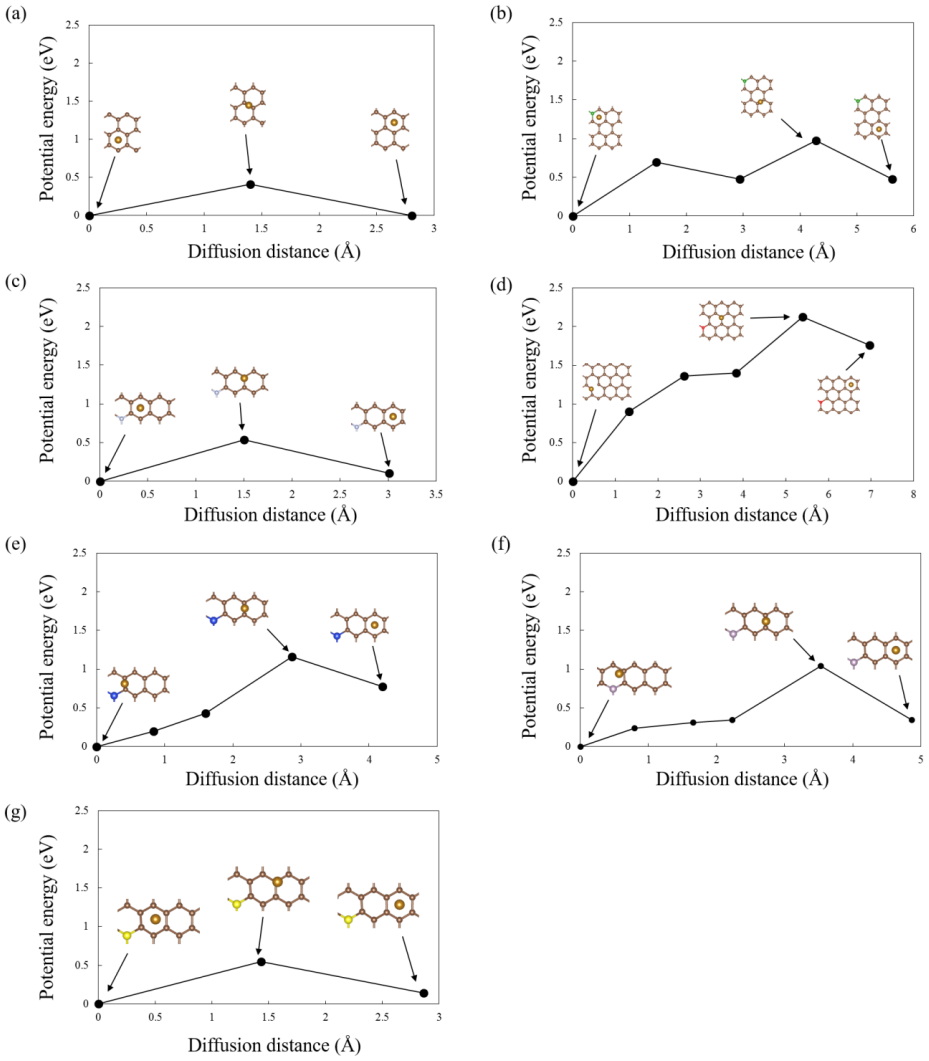

FIG. 11. Potential energy change of Fe atoms as a function of diffusion distance on (a) pristine graphene and (b) B-, (c) N-, (d) O-, (e) Si-, (f) P-, and (g) S-doped graphene. The origin of potential energy is set to the total energy at the most stable adsorption site for the Fe atom. The insets show the atomic configurations involved in the diffusion of Fe atoms.

This indicates that the dopants can easily trap Fe atoms. From the adsorption energy and diffusion barrier results, we conclude that B-, O-, Si-, and P-doped graphene are promising supports for suppressing Fe detachment and agglomeration.

IV. CONCLUSION

We investigated the adsorption states and diffusion behavior of a single Fe atom on light-element-doped graphene, using first-principles calculations based on spin-polarized DFT. In comparison with pristine graphene, Fe atoms adsorb strongly on light-element-doped graphene, because localized orbitals are created in the vicinity of the dopants. This strong adsorption suppresses Fe detachment. In terms of Fe diffusion behavior, the diffusion barriers of Fe atoms on light-element-doped graphene are larger than that on pristine graphene. In particular, B-, O-, Si-, and P-doped graphene show large diffusion barriers, which suppresses Fe atom diffusion and agglomeration. This suggest that B, O, Si, and P doping into

graphene could improve the durability of Fe nanocluster catalysts. Understanding the adsorption and diffusion behavior discussed herein may help to improve the durability of various metal clusters.

ACKNOWLEDGMENTS

This work was supported by MEXT KAKENHI: Grant-in-Aid for Scientific Research on Innovative Areas, Japan (Grant No. JP16H00928). This work was carried out using the facilities of the Supercomputer Center, Institute for Solid State Physics, University of Tokyo, Japan.

[1] L. Schlapbach and A. Züttel, Nature **414**, 353 (2001).
[2] W. Zhou, J. Zhou, J. Shen, C. Ouyang, and S. Shi, J. Phys. Chem. Solids **73**, 245 (2012).
[3] Z. M. Ao and F. M. Peeters, Phys. Rev. B **81**, 205406 (2010).
[4] A. Bhattacharya, S. Bhattacharya, C. Majumder, and G. P. Das, J. Phys. Chem. C **114**, 10297 (2010).
[5] A. Reyhani, S. Z. Mortazavi, S. Mirershadi, A. Z. Moshfegh, P. Parvin, and A. N. Golikand, J. Phys. Chem. C **115**, 6994 (2011).
[6] K. Takahashi, S. Isobe, and S. Ohnuki, Appl. Phys. Lett. **102**, 113108 (2013).
[7] J. V. Badding, R. J. Hemley, and H. K. Mao, Science **253**, 421 (1991).
[8] T. Suzuki, S. Akimoto, and Y. Fukai, Phys. Earth Planet. Inter. **36**, 135 (1984).
[9] V. E. Antonov, I. T. Belash, V. F. Degtyareva, D. N. Mogilyansky, B. K. Ponomarev, and V. S. Shekhtman, Int. J. Hydrogen Energy **14**, 371 (1989).
[10] N. Ishimatsu, T. Shichijo, Y. Matsushima, H. Maruyama, Y. Matsuura, T. Tsumuraya, T. Shishidou, T. Oguchi, N. Kawamura, M. Mizumaki, T. Matsuoka, and K. Takemura, Phys. Rev. B **86**, 104430 (2012).
[11] M. Sterlin Leo Hudson, H. Raghubanshi, S. Awasthi, T. Sadhaivam, A. Bhatnager, S. Simizu, S. G. Sankar, and O. N. Srivastava, Int. J. Hydrogen Energy **39**, 8311 (2014).
[12] K. Takahashi, Y. Wang, S. Chiba, Y. Nakagawa, S. Isobe, and S. Ohnuki, Sci. Rep. **4**, 4598 (2014).
[13] H. Peng, Z. Mo, S. Liao, H. Liang, L. Yang, F. Luo, H. Song, Y. Zhong, and B. Zhang, Sci. Rep. **3**, 1765 (2013).
[14] K. Parvez, S. Yang, Y. Hernandez, A. Winter, A. Turchanin, X. Feng, and K. Müllen, ACS Nano **6**, 9541 (2012).
[15] L. S. Zhang, X. Q. Liang, W. G. Song, and Z. Y. Wu, Phys. Chem. Chem. Phys. **12**, 12055 (2010).
[16] B. P. Vinayan, R. Nagar, N. Rajalakshmi, and S. Ramaprabhu, Adv. Funct. Mater. **22**, 3519 (2012).
[17] T. Holme, Y. Zhou, R. Pasquarelli, and R. O'Hayre, Phys. Chem. Chem. Phys. **12**, 9461 (2010).
[18] J. Park, Y. J. Jang, Y. J. Kim, M. Song, S. Yoon, D. H. Kim, and S. J. Kim, Phys. Chem. Chem. Phys. **16**, 103 (2014).
[19] G. Kresse and J. Hafner, Phys. Rev. B **47**, 558(R) (1993).
[20] G. Kresse and J. Hafner, Phys. Rev. B **49**, 14251 (1994).
[21] G. Kresse and J. Furthmüller, Phys. Rev. B **54**, 11169 (1996).
[22] G. Kresse and J. Furthmüller, Comput. Mater. Sci. **6**, 15 (1996).
[23] G. Kresse and D. Joubert, Phys. Rev. B **59**, 1758 (1999).
[24] P. E. Blöchl, Phys. Rev. B **50**, 17953 (1994).
[25] J. P. Perdew, K. Burke, and M. Ernzerhof, Phys. Rev. Lett. **77**, 3865, (1996).
[26] J. D. Pack and H. J. Monkhorst, Phys. Rev. B **16**, 1748 (1977).
[27] S. Hasegawa, Y. Kunisada, and N. Sakaguchi, J. Phys. Chem. C **121**, 17787 (2017).
[28] G. Makov and M. Payne, Phys. Rev. B **51**, 4014 (1995).
[29] J. Neugebauer and M. C. Scheffler, Phys. Rev. B. **46**, 16067 (1992).
[30] G. Henkelman, A. Arnaldsson, and H. Jónsson, Comput. Mater. Sci. **36**, 354 (2006).
[31] W. Tang, E. Sanville, and G. Henkelman, J. Phys.: Condens. Matter **21**, 084204 (2009).
[32] R. F. W. Bader, Chem. Rev. **91**, 893 (1991).
[33] S. Maintz, M. Esser, and R. Dronskowski, Acta Physica Polonica B **47**, 1165 (2016).
[34] V. L. Deringer, A. L. Tchougréeff, and R. Dronskowski, J. Phys. Chem. A **115**, 5461 (2011).
[35] K. Momma and F. Izumi, J. Appl. Crystallogr. **44**, 1272 (2011).
[36] H. Sevinçli, M. Topsakal, E. Durgun, and S. Ciraci, Phys. Rev. B **77**, 195434 (2008).
[37] K. T. Chan, J. B. Neaton, and M. L. Cohen, Phys. Rev. B **77**, 235430 (2008).
[38] H. Valencia, A. Gil, and G. Frapper, J. Phys. Chem. C **114**, 14141 (2010).